Braun, M., Iváñez, I. (2020). Numerical study of damaged micro-lattice blocks subjected to uniaxial compressive loading. *Extreme Mechanics Letters*, v. 39: 100821, pp.: 1-8.

DOI: https://doi.org/10.1016/j.eml.2020.100821

Numerical study of damaged micro-lattice blocks subjected to uniaxial compressive loading

M. Braun[a,b,*], I. Iváñez[c]

[a] *Departamento de Construcciones, Facultad de Ingeniería, Universidad Nacional de La Plata, Avda. 1 esq. 47, La Plata B1900TAG, Argentina*
[b] *Consejo Nacional de Investigación Científicas y Técnicas (CONICET), CCT La Plata, Calle 8 N° 1467, La Plata B1904CMC, Argentina*
[c] *Department of Continuum Mechanics and Structural Analysis University Carlos III of Madrid. Avda. de la Universidad, 30. 28911 Leganés, Madrid, Spain*

Abstract

This article presents a numerical study on the mechanical behaviour of damaged micro-lattice (ML) blocks submitted to uniaxial compressible loads. The numerical model is implemented in the commercial finite-element code Abaqus/Standard. From the finite-element model, the initial stiffness and the Yield stress of ML blocks are calculated. The damage in ML blocks is modelled as manufacturing defects, that are included in the ML structures using a random algorithm implemented in MatLab. The numerical model is validated with experimental data from uniaxial compression tests carried out on ML intact blocks by other authors. The analysis of the mechanical behaviour of ML blocks is presented in terms of variations of damage percentage, cell type and cell size.

Keywords: Micro-Lattice, Mechanical Properties, Damage, Finite Element

*Corresponding author. Tel. +54 221 4258911; Fax: +54 221 4258911. E-mail address: matias.braun@ing.unlp.edu.ar

1. Introduction

In the last decades, the advance on additive manufacturing techniques allowed developing new materials based on periodic structures [1, 2]. The additive manufacturing has the greatest flexibility in realising fully bespoke three–dimensional solutions [3, 4, 5].

Some issues included conformal lattice structures, in which the lattice structures follow curved contours, and graded lattice structures, to fully optimize the distribution of structurally effective material. Furthermore, the three–dimensional lattice structures induce axial forces in the individual members, so it is expected to have a high specific stiffness per unit weight [6]. Their mechanical properties make them attractive to be used as cores in sandwich structures [7, 8, 9, 10].

Researchers from the University of Liverpool developed an additive manufacturing process to produce micro-lattice structures. This process is based on a selective laser melting (SLM) system, and it permits to manufacture lattice structures with high complexity which can be built at the micrometre scale in relatively short times [11]. In this regard, numerous works present experimental results [12, 13, 14, 15, 16, 17] of the mechanical responses of micro-lattice structures submitted to different loadings and boundary conditions.

In the same way, several researches [18, 19, 20, 21, 22] developed numerical and analytical studies on the compressive strengths and the initial stiffness of open cell materials. The work presented by Smith *et al.* [22] showed

that predictions obtained using beam elements in finite-element models are capable of obtaining the stiffness and Yield stress of ML structures submitted to compression loads. In their work, they presented a numerical analysis, validated with experimental results of cubic ML blocks manufactured using SLM system.

However, being this system a complex process, it will be most susceptible to imperfections in the form of inherent micro-voids due to the stacking–layered fused nature of the metal powder [23, 24, 25, 26, 27, 28, 29, 30, 31]. Recently, it has been proved that the presence of imperfections in ML structures produces changes in their vibrational response [32].

The aim of this work is to study the mechanical response of damaged ML blocks submitted to uni-axial compressible loads. A finite-element model implemented in the commercial software Abaqus/Standard [33] is used to calculate the stiffness and the Yield stress of intact and damaged ML cubes. In order to study the influence of imperfections on the mechanical behaviour of ML structures, members (struts) of the ML structure are removed using an algorithm implemented in MatLab. Finally, the numerical model is validated with experimental data of uni-axial compression tests on ML intact blocks presented by other authors [22]. The influence of the damage percentage in terms of cell type and cell size on the mechanical properties of ML blocks is analysed.

2. Description of the problem

The problem considered in this work is based on the experimental work presented in [22], in which the authors tested cubic ML blocks under quasi-

static compression loads. The blocks were manufactured with the SLM technique, using 316L stainless steel. The plates of the test machine were greased before each test to reduce any friction between the plates and the cubes.

In the present study, two unit-cell topologies of ML structure are considered: a body-centred cubic arrangement (BCC), and the same structure with vertical bars (BCC-Z). Fig.1 shows a schematic representation of both cell topologies. The cell size is defined by the parameter h. Note that the BCC-Z ML cubes were compressed in the direction of the vertical pillars.

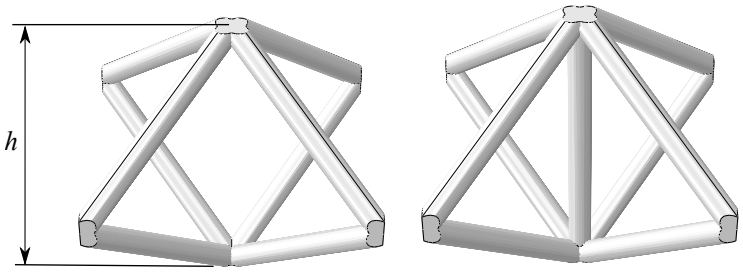

(a) BCC unit cell. (b) BCC-Z unit cell.

Figure 1: Configurations of the unit cells.

3. Numerical model

Fig. 2 shows perspective and front views of the developed numerical model, in which the ML cube and the plates of the load machine are modelled. Both plates are defined as rigid shell and are meshed using quadrilateral elements of 0.5 mm in size.

The ML structure is discretised using Euler-Bernoulli beams (B33 - simple 2-node beam elements) available in Abaqus/Standard library. These el-

ements do not allow a transverse shear deformation to occur; plane sections initially normal to the beam's axis remain plane and normal to the beam axis. The work presented by Smith *et al.* [22] showed that the quasi-static response of ML structures can be described using beam element types. The geometry is simplified, so the struts were represented by straight beams with a circular cross-section of a 0.20 mm constant diameter.

The mechanical behaviour of ML bars is modelled with an elastic-plastic constitutive model, with the following material properties: Young's modulus $E = 140$ GPa, Poisson's ratio $\nu = 0.27$, Yield strength $\sigma_y = 144$ MPa, and density $\rho = 7870$ kg/m^3 [34, 13].

A mesh sensitivity analysis was performed in order to find a good balance between accuracy and computational costs. The analysis was focused on the results of the initial part of the stress-strain curve obtained from the simulations, which shows a good correlation with experimental data when only one B33 element per member is used. The finite-element mesh of BCC ML structures contained approximately 14398, 36846 and 48576 elements for cell sizes of 2.50, 1.67 and 1.25 mm, respectively.

The contact between plates and the ML cube was assumed as *hard contact* (using penalty constraint enforcement) in the normal direction and *frictionless* in the tangential direction.

Because of their manufacturing process, ML structures can present defects and imperfections, such as variable cross -section, wavy struts and micropores [35]. These defects can cause premature failure of defective struts. The aim of this paper is to explore the sensitivity of both Young's modulus and Yield strength to the presence of defects. Imperfections are limited to

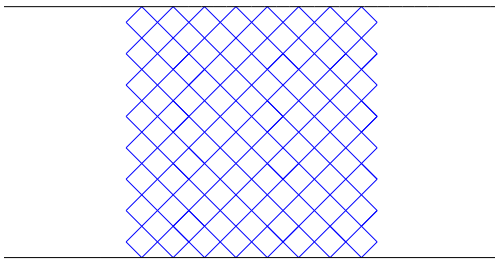

(a) Front view.

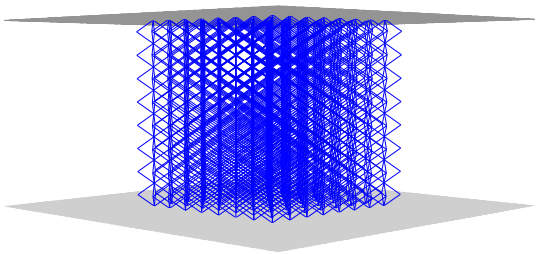

(b) Perspective view.

Figure 2: Geometry of the numerical model.

randomly missing struts, as prior studies suggest that displaced nodes and missing cell walls rapidly knock down the strength of lattices [36]. Therefore, the most restrictive hypothesis to simulate damage is the total disappearance of struts.

In this context, the presence of defects as damage in the ML structure is defined with an algorithm programmed in MatLab language. The developed MatLab code randomly removes members (struts) of the ML structure. These elements are incorporated within the Abaqus input file, assigning new material properties with null stiffness. Five ML structures of each cell type and size were virtually tested in order to obtain the average and the standard

deviation of the numerically determined mechanical properties.

4. Validation of the numerical model

This section presents the validation of the numerical model with the experimental data taken from the literature for intact ML structures [22]. For the sake of brevity, only intact ML blocks with cell sizes of 2.50 and 1.25 mm for both BCC and BCC-Z cell types were modelled.

Tables 1 and 2 show the numerical and experimental values of Young's modulus and Yield stress obtained for each case, respectively. The experimental results and the percent errors of the numerical model are included.

The deviation of numerical predictions with respect to experimental values is less than 16%, and the order of magnitude of the numerical values is the same as that of the experimental data.

Cell type	Size [mm]	Experimental [MPa]	Numerical [MPa]	Error [%]
BCC	2.50	10.60	12.10	14.2
	1.25	207.50	238.90	15.1
BCC-Z	2.50	547.20	478.05	12.6
	1.25	2273.20	2166.59	4.7

Table 1: Experimental [22] and numerical values of Young's modulus.

Cell type	Size [mm]	Experimental [MPa]	Numerical [MPa]	Error [%]
BCC	2.50	0.16	0.18	12.5
	1.25	2.56	2.15	16.0
BCC-Z	2.50	1.04	1.07	2.9
	1.25	7.02	5.95	15.2

Table 2: Experimental [22] and numerical values of Yield stress.

Furthermore, a representative stress-strain curve for BCC model (2.50 mm in size) is presented and compared with experimental data in Fig. 3. In both curves there is a sharp rise in the elastic region followed by a stress plateau. This behaviour has been reported for cellular foam structures. The numerical model captures the initial stiffness (Young's modulus) and Yield stress values experimentally observed in [22], and results show good correlation in the first part of the curve. In this way, the curve can be characterised by Young's modulus and Yield stress.

The numerical results are reasonably consistent with those of the experimental measurements taken from the literature, thus the model is used for further analysis on the comparison of the mechanical behaviour of damaged ML blocks when subjected to compressive loads.

The numerical model allows a better understanding of the failure modes of the simulated structures. In this regard, Fig. 4 presents a qualitative comparison of the deformation modes of BCC and BCC-Z ML blocks, respectively. The numerical failure modes (b) are compared with the experimental data (a) presented in the work by Gümruk *et al* [16]. The numerical models

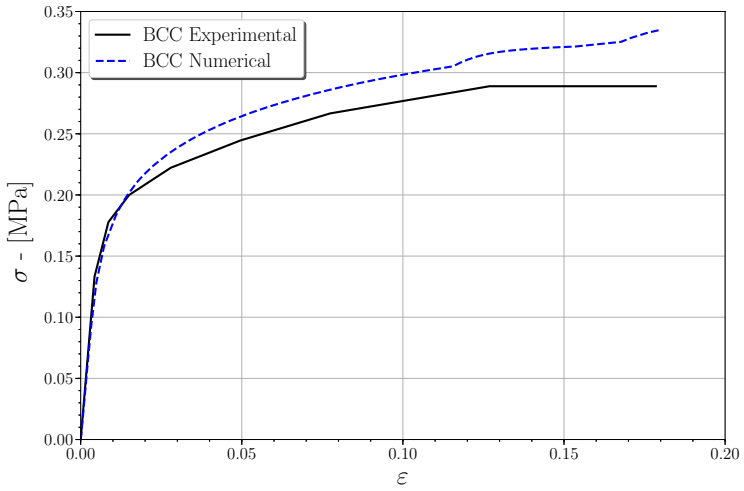

Figure 3: Numerical and experimental [22] stress-strain curves for BCC configuration (cell size of 2.50 mm).

capture the shear band formation, that is oriented at an inclination angle of 45°. Note that these local deformations begin at the corners of the ML structure, growing towards the inside of the ML block.

5. Results and discussion

5.1. Non-damage analysis

Fig. 5 shows the numerical results of intact ML blocks, the two cell configurations BCC and BCC-Z and three different sizes (2.50, 1.67 and 1.25 mm). For both Young's modulus and Yield stress results, the trend is exactly the same: values for BCC-Z structures are greater than those obtained for BCC cells. This might be due to the presence of the central pillar in the cell type BCC-Z, which provides more stability against buckling.

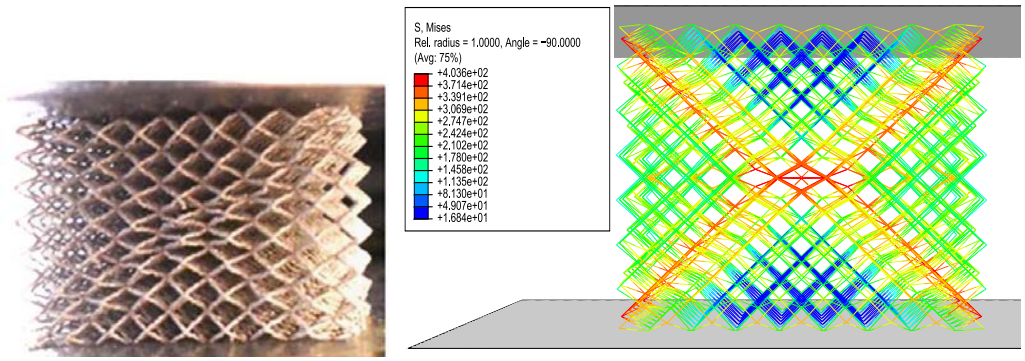

(a) BCC Experimental data.

(b) Von Mises field stress of the BCC block.

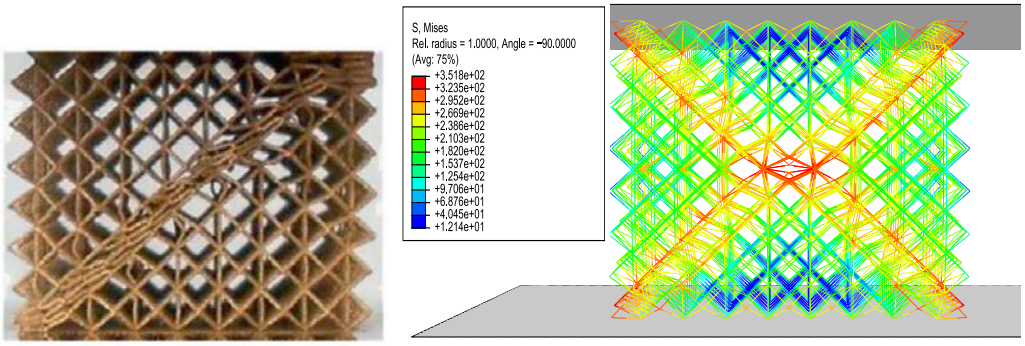

(c) BCC-Z Experimental data.

(d) Von Mises field stress of the BCC-Z block.

Figure 4: Numerical and experimental [16] results of the BCC and BCC-Z blocks for cell size of 2.5 mm.

The trend is also the same when results are analysed as a function of the cell size: both Young's modulus and Yield stress decrease in ML blocks with larger cell sizes. This behaviour is also given for honeycomb structures: smaller cell sizes share some properties with homogeneous structures, as the cross-sectional area in which the compression load is distributed is greater than in structures with larger cell sizes [37]. In addition, larger cell sizes, when compressed, take longer to come into contact with each other, present-

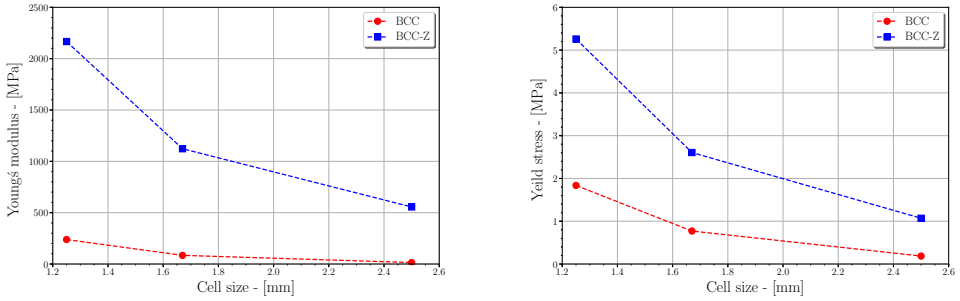

(a) Young's modulus (b) Yield stress

Figure 5: Numerical results of non-damaged (intact) micro-lattice structures.

ing lower stiffness.

The results of non-damaged (intact) ML blocks will be used to assess the mechanical properties of ML structures as a function of the damage level.

5.2. Damage effect on Young's modulus

In order to analyse the effect of the damage location, five random cases for each damage percent were considered in the analysis. Tables 3 and 4 present the values of the average Young's modulus and the standard deviation for BCC and BCC-Z cells, respectively. The maximum percent of standard deviation for BCC cell is 2.16%, while BCC-Z cell has a maximum percent standard deviation of 9.33%. Therefore, BCC-Z cell presents an upper dependence on the damage localization than BCC cell.

Damage	2.5 mm		1.66 mm		1.25 mm	
[%]	E [MPa]	s	E [MPa]	s	E [MPa]	s
0	14.35	0	84.41	0	238.33	0
5	13.61	0.07	78.70	0.24	221.82	0.53
10	12.88	0.10	72.84	0.26	205.68	0.53
15	11.99	0.14	67.15	0.27	189.57	0.53
20	11.20	0.17	61.40	0.71	174.02	0.98
25	10.24	0.05	55.62	0.52	158.75	1.08
30	9.32	0.12	50.50	0.33	144.52	0.73
35	8.39	0.16	45.12	0.29	130.73	1.29
40	7.65	0.17	40.69	0.24	117.93	0.88

Table 3: Mean Young's modulus and standard deviation values for BCC cell.

Damage	2.5 mm		1.66 mm		1.25 mm	
[%]	E [MPa]	s	E [MPa]	s	E [MPa]	s
0	555.76	0	1122.79	0.00	2166.59	0
5	440.51	3.21	1044.23	6.83	2014.95	8.92
10	378.73	35.35	963.47	17.04	1869.75	11.19
15	358.47	12.04	883.49	7.97	1715.61	13.79
20	331.79	10.21	801.70	8.28	1564.87	13.22
25	276.97	16.26	708.99	32.04	1419.97	15.37
30	248.06	7.23	634.50	22.49	1266.78	20.37
35	212.93	18.14	552.91	20.43	1110.15	14.03
40	169.35	15.04	463.20	9.59	970.93	35.62

Table 4: Mean Young's modulus and standard deviation values for BCC-Z cell.

Fig. 6(a) and 6(b) present the numerical results of normalised Young's modulus as a function of the damage generated through the algorithm implemented in Matlab. The results have been normalised with the value obtained for numerical intact ML blocks, thus it is possible to estimate the variation of stiffness with increasing damage in these structures. Note that the normalised Young's modulus is calculated from the average values presented in Tables 3 and 4.

In ML structures composed by BCC cells, Young's modulus decreases almost linearly with respect to the intact value for the three sizes studied. BCC cells of 1.25 and 1.67 mm show similar results, and the curves practically overlap for all damage percentages. Differences among both cell sizes results and those of cell size 2.50 mm become more noticeable in a damage percentage of 10%. However, differences among the results of the three cell sizes do not present variations greater than 6%. For BCC cells, the variation of Young's modulus between intact ML blocks (0%) and the highest percentage of damage (40%) is approximately 50%.

Results for ML structures with BCC-Z cells present more differences when represented as a function of cell size. Results for BCC-Z cell sizes of 1.25 and 1.67 mm practically overlap until a damage level of 20%, as observed in BCC cells. From that point, differences between both sizes do not exceed 5%. The reduction of the normalised Young's modulus as a function of damage level is almost linear, reaching values of 0.4-0.45 for a damage level of 40%, which are slightly lower when compared to those obtained from BCC cell blocks.

On the other hand, the trend of the curve given for ML blocks with cell size of 2.50 mm shows more differences in BCC-Z cells: for the lowest per-

centage of damage (5%) the drop in Young's modulus values, when compared to the other cell sizes, is much greater than in BCC blocks (difference being approximately 15%), and 20% with respect to Young's modulus of the intact ML block. For 10% damage, this drop starts to soften, and from a damage level of 15%, the curve ends up showing a similar slope to the one given by the other two sizes.

As the initial drop is much more pronounced in cells of 2.50 mm, for a damage level of 40% the stiffness decreased from the initial value to 70%. This behaviour indicates that ML blocks with BCC-Z arrangements are more affected by the damage generation than by ML blocks with BCC cells, as it was suggested in results of Table 4.

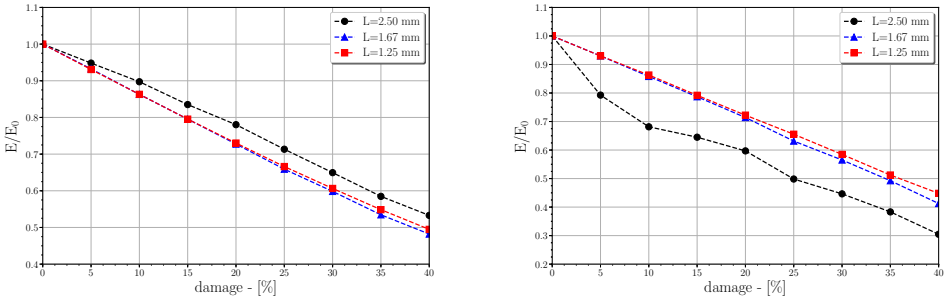

(a) BCC ML block.

(b) BCC-Z ML block.

Figure 6: Normalised Young's modulus as a function of damage level.

5.3. Damage effect on Yield stress

Similarly to the previous section, five random cases for each damage percent were considered in order to study the variation of Yield stress. Tables

5 and 6 present the values of the mean Yield stress and the standard deviation for BCC and BCC-Z cell, respectively. The standard deviation of Yield stress presents the same tendency that Young's modulus, where the BCC-Z cell has an upper dependence on the damage position than the BCC cell. In this case, the maximum values of the percent standard deviation are 2.30 and 7.29 percent for BCC and BCC-Z cell, respectively.

Damage	2.5 mm		1.66 mm		1.25 mm	
[%]	$\sigma_{0.2}$ [MPa]	s	$\sigma_{0.2}$ [MPa]	s	$\sigma_{0.2}$ [MPa]	s
0	0.1865	0	0.7707	0	1.8362	0
5	0.1718	0.0007	0.7157	0.0067	1.6810	0.0038
10	0.1634	0.0026	0.6575	0.0077	1.5293	0.0036
15	0.1502	0.0017	0.5994	0.0061	1.4384	0.0039
20	0.1363	0.0022	0.5622	0.0032	1.3053	0.0215
25	0.1243	0.0020	0.5081	0.0048	1.1864	0.0067
30	0.1118	0.0026	0.4620	0.0029	1.0910	0.0097
35	0.0990	0.0028	0.4136	0.0023	0.9888	0.0070
40	0.0902	0.0019	0.3740	0.0020	0.9025	0.0067

Table 5: Mean Yield stress and standard deviation values for BCC cell.

Damage	2.5 mm		1.66 mm		1.25 mm	
[%]	$\sigma_{0.2}$ [MPa]	s	$\sigma_{0.2}$ [MPa]	s	$\sigma_{0.2}$ [MPa]	s
0	1.0700	0	2.6055	0	5.2595	0
5	1.0148	0.0180	2.5268	0.0431	4.8914	0.0198
10	0.9574	0.0168	2.3372	0.0508	4.5440	0.0229
15	0.8878	0.0162	2.1781	0.0155	4.1841	0.0293
20	0.8182	0.0199	1.9919	0.0157	3.8409	0.0309
25	0.7065	0.0243	1.7737	0.0463	3.5094	0.0310
30	0.6380	0.0134	1.6171	0.0548	3.1649	0.0404
35	0.5597	0.0320	1.4338	0.0462	2.8173	0.0285
40	0.4598	0.0335	1.2220	0.0228	2.5031	0.0771

Table 6: Mean Yield stress and standard deviation values for BCC-Z cell.

Fig. 7(a) and 7(b) represent the normalised Yield stress as a function of the damage level. The Yield stress in the numerical model is chosen as the stress that causes a permanent strain of 0.002 in the ML structure ($\varepsilon = 0.2$). The normalised Yield stress presented in Fig. 7 is defined as the ratio between the Yield stress obtained in the numerical simulations, which depends on the selected damage level, and the Yield stress value given by intact ML blocks.

In general, Yield stress linearly decreases with the increasing damage level. In the case of ML blocks composed by BCC cells, Yield stress decreases by 50% for a damage of 40% when compared to intact blocks. For the three cell sizes (2.50, 1.67 and 1.25 mm), the decrease slope is practically the same. However, for a damage level between 5% and 30%, there are slight differences between the three curves and ML blocks with larger cells (2.50 mm) which

values of Yield stress slightly higher than those of smaller cells.

For BCC-Z cells the results are similar: the three curves linearly decay with a similar slope, presenting a decrease in Yield stress of around 55% between intact blocks and blocks with a 40% damage. In this case, the curves for the three cell sizes show more differences from the beginning of the damage inclusion, and larger cells have a Yield stress value slightly higher than that of ML blocks with smaller cell sizes. However, from a damage level of 25% the Yield stress of the largest cell size (2.50 mm) decreases with respect to the results given by the other two cell sizes.

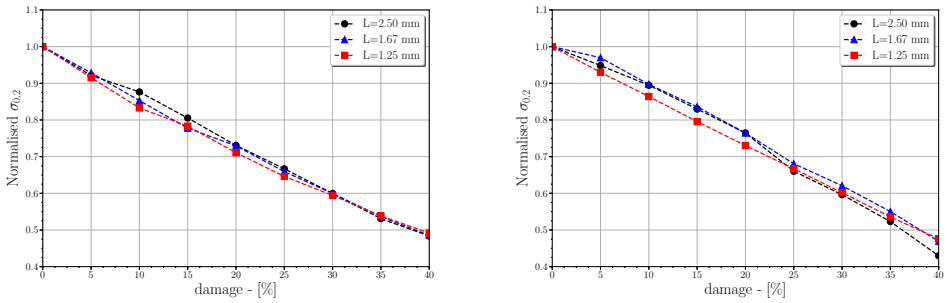

(a) BCC ML block.

(b) BCC-Z ML block.

Figure 7: Normalised Yield stress as a function of damage level.

5.4. Damage effect as a function of the cell type

Fig. 8 shows the comparison of the variation of Young's modulus for the three cell sizes studied as a function of the cell type unit (BCC and BCC-Z).

Results for cells of 1.67 mm and 1.25 mm are practically the same, thus the cell type has no visible effect on the stiffness of the ML blocks. In cells of 1.67 mm in size, the results between BCC and BCC-Z cells almost overlap

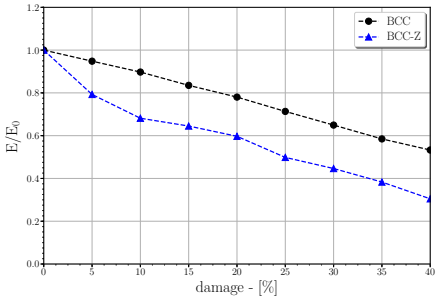

(a) L= 2.5 mm.

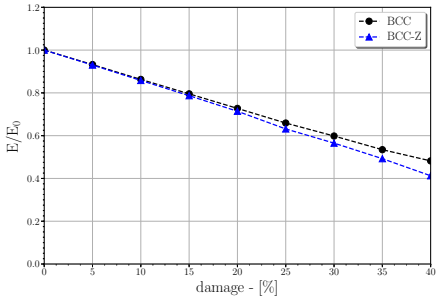

(b) L= 1.67 mm.

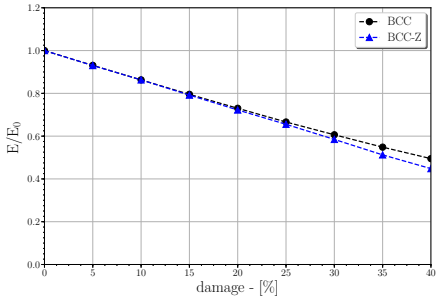

(c) L= 1.25 mm.

Figure 8: Normalised Young's modulus in function of damage level for different cell types.

until a damage level of 10% is reached. From that point, the value of the Young's modulus is slightly higher for BCC-Z cells. The same trend can be observed at cells of 1.25 mm, only that the curves begin to show their differences from a damage level of 15%.

Differences between BCC and BCC-Z cells for cell sizes of 2.50 mm is noticeable from the beginning of damage inclusion. The decrease in Young's modulus is more visible in ML blocks with BCC-Z cells than in blocks with BCC arrangements. Therefore, the loss of the vertical pillar that differ-

entiates BCC-Z cells from BCC notably affects the stiffness of ML blocks. Moreover, Yield stress does not display significant differences when depicted as a function of the cell type (Fig.9), and differences are negligible in all three cases.

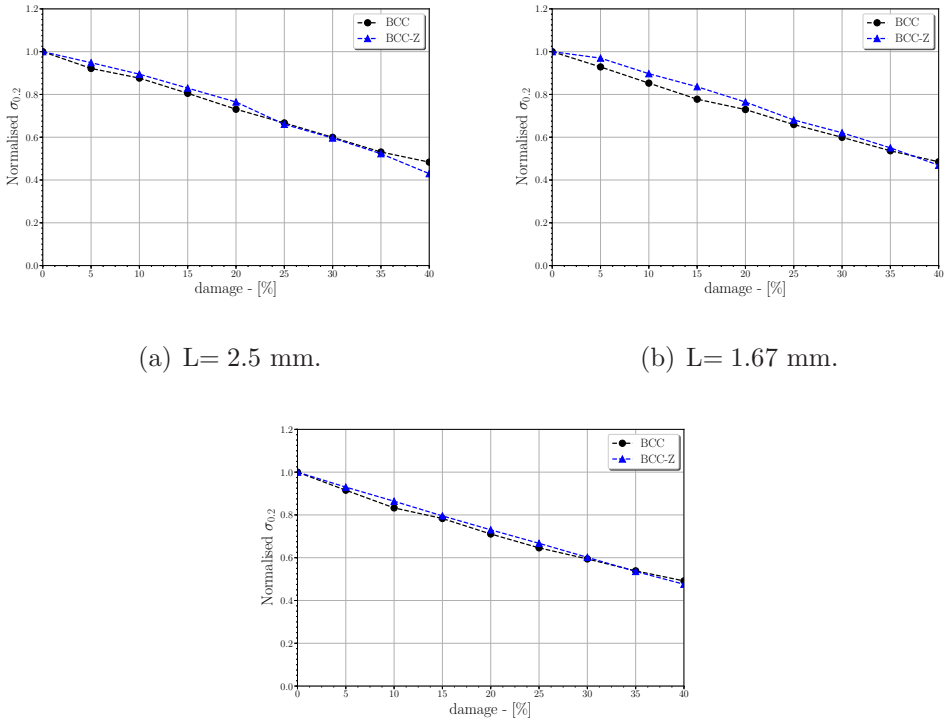

(a) L= 2.5 mm.

(b) L= 1.67 mm.

(c) L= 1.25 mm.

Figure 9: Normalised Yield stress in function of damage level for different cell types

As a conclusion, it is Young's modulus (and therefore, the stiffness of the ML structure) the most relevant parameter to take into account when choosing the cell type in the ML blocks design.

6. Conclusions

In this work, a finite-element model was implemented to study the mechanical response of micro-lattice metallic blocks submitted to compressive loads. The simulations are focused on showing the sensitivity of the mechanical properties to the presence of defects (damage) in the micro-lattice block. In this context, a MatLab code was developed to generate the geometry and the random defects in the simulated ML blocks.

Firstly, the numerical model was validated with experimental results obtained from intact blocks. In this way, two cell sizes were studied for both BCC and BCC-Z cells arrangements. The results showed that the numerical model is capable of predicting Young's modulus and Yield stress with a relative error lower than 16%.

The numerical model allowed studying the effect of the damage level on the mechanical properties. The normalised values of Young's modulus and Yield stress linearly decrease with the same slope when the damage increases (for all cell sizes and types). Therefore, the damage presence generates the same effect on the mechanical properties, independently of cell type or size. However, BCC-Z cells have upper dependence on the location of damage than BCC cell.

Acknowledgments

The authors wish to gratefully acknowledge the financial support of the Spanish Ministry of Economy and Competitiveness under Projects DPI2011-24068 and DPI2011-23191.

References

[1] S. Yang, Y. F. Zhao, Additive manufacturing-enabled design theory and methodology: a critical review, The International Journal of Advanced Manufacturing Technology 80 (1-4) (2015) 327–342.

[2] X. An, C. Lai, W. He, H. Fan, Three-dimensional meta-truss lattice composite structures with vibration isolation performance, Extreme Mechanics Letters 33 (2019) 100577.

[3] M. Rashed, M. Ashraf, R. Mines, P. J. Hazell, Metallic microlattice materials: A current state of the art on manufacturing, mechanical properties and applications, Materials & Design 95 (2016) 518–533.

[4] Y. He, Y. Zhou, Z. Liu, K. Liew, Buckling and pattern transformation of modified periodic lattice structures, Extreme Mechanics Letters 22 (2018) 112 – 121.

[5] M. A. Wagner, T. S. Lumpe, T. Chen, K. Shea, Programmable, active lattice structures: Unifying stretch-dominated and bending-dominated topologies, Extreme Mechanics Letters 29 (2019) 100461.

[6] D. T. Queheillalt, H. N. Wadley, Titanium alloy lattice truss structures, Materials & Design 30 (6) (2009) 1966–1975.

[7] J. Wallach, L. Gibson, Mechanical behavior of a three-dimensional truss material, International Journal of Solids and Structures 38 (40-41) (2001) 7181–7196.

[8] D. J. Sypeck, Cellular truss core sandwich structures, Applied Composite Materials 12 (3-4) (2005) 229–246.

[9] K. Wei, Q. Yang, B. Ling, H. Xie, Z. Qu, D. Fang, Mechanical responses of titanium 3d kagome lattice structure manufactured by selective laser melting, Extreme Mechanics Letters 23 (2018) 41 – 48.

[10] H. C. Tankasala, N. A. Fleck, The crack growth resistance of an elastoplastic lattice, International Journal of Solids and Structures 188-189 (2020) 233 – 243.

[11] O. Rehme, Cellular design for laser freeform fabrication, Cuvillier Göttingen, 2010.

[12] R. Hasan, R. Mines, S. Tsopanos, Determination of elastic modulus value for selectively laser melted titanium alloy micro-struty, Journal of Mechanical Engineering and Technology (JMET) 2 (2) (2010).

[13] S. Tsopanos, R. Mines, S. McKown, Y. Shen, W. Cantwell, W. Brooks, C. Sutcliffe, The influence of processing parameters on the mechanical properties of selectively laser melted stainless steel microlattice structures, Journal of Manufacturing Science and Engineering 132 (4) (2010) 041011.

[14] Y. Shen, S. McKown, S. Tsopanos, C. Sutcliffe, R. Mines, W. Cantwell, The mechanical properties of sandwich structures based on metal lattice architectures, Journal of Sandwich Structures & Materials 12 (2) (2010) 159–180.

[15] R. Hasan, R. Mines, P. Fox, Characterization of selectively laser melted ti-6al-4 v micro-lattice struts, Procedia Engineering 10 (2011) 536–541.

[16] R. Gümrük, R. Mines, S. Karadeniz, Static mechanical behaviours of stainless steel micro-lattice structures under different loading conditions, Materials Science and Engineering: A 586 (2013) 392–406.

[17] R. Mines, S. Tsopanos, Y. Shen, R. Hasan, S. McKown, Drop weight impact behaviour of sandwich panels with metallic micro lattice cores, International Journal of Impact Engineering 60 (2013) 120–132.

[18] H. Zhu, J. Knott, N. Mills, Analysis of the elastic properties of open-cell foams with tetrakaidecahedral cells, Journal of the Mechanics and Physics of Solids 45 (3) (1997) 319–343.

[19] L. J. Gibson, M. F. Ashby, Cellular solids: structure and properties, Cambridge university press, 1999.

[20] M. H. Luxner, J. Stampfl, H. E. Pettermann, Finite element modeling concepts and linear analyses of 3d regular open cell structures, Journal of Materials science 40 (22) (2005) 5859–5866.

[21] G. Labeas, M. Sunaric, Investigation on the static response and failure process of metallic open lattice cellular structures, Strain 46 (2) (2010) 195–204.

[22] M. Smith, Z. Guan, W. Cantwell, Finite element modelling of the compressive response of lattice structures manufactured using the selective laser melting technique, International Journal of Mechanical Sciences 67 (2013) 28–41.

[23] X. Zhao, S. Li, M. Zhang, Y. Liu, T. B. Sercombe, S. Wang, Y. Hao, R. Yang, L. E. Murr, Comparison of the microstructures and mechanical properties of ti–6al–4v fabricated by selective laser melting and electron beam melting, Materials & Design 95 (2016) 21–31.

[24] H. Gong, K. Rafi, H. Gu, G. J. Ram, T. Starr, B. Stucker, Influence of defects on mechanical properties of ti–6al–4 v components produced by selective laser melting and electron beam melting, Materials & Design 86 (2015) 545–554.

[25] A. Bauereiß, T. Scharowsky, C. Körner, Defect generation and propagation mechanism during additive manufacturing by selective beam melting, Journal of Materials Processing Technology 214 (11) (2014) 2522–2528.

[26] Q. C. Liu, J. Elambasseril, S. J. Sun, M. Leary, M. Brandt, P. K. Sharp, The effect of manufacturing defects on the fatigue behaviour of ti-6al-4v specimens fabricated using selective laser melting, in: Advanced Materials Research, Vol. 891, Trans Tech Publ, 2014, pp. 1519–1524.

[27] S. Leuders, M. Thöne, A. Riemer, T. Niendorf, T. Tröster, H. Richard, H. Maier, On the mechanical behaviour of titanium alloy tial6v4 manufactured by selective laser melting: Fatigue resistance and crack growth performance, International Journal of Fatigue 48 (2013) 300–307.

[28] X. Zhou, D. Wang, X. Liu, D. Zhang, S. Qu, J. Ma, G. London, Z. Shen, W. Liu, 3d-imaging of selective laser melting defects in a co–cr–mo alloy by synchrotron radiation micro-ct, Acta Materialia 98 (2015) 1–16.

[29] S. Siddique, M. Imran, E. Wycisk, C. Emmelmann, F. Walther, Influence of process-induced microstructure and imperfections on mechanical properties of alsi12 processed by selective laser melting, Journal of Materials Processing Technology 221 (2015) 205–213.

[30] S. Tammas-Williams, H. Zhao, F. Léonard, F. Derguti, I. Todd, P. Prangnell, Xct analysis of the influence of melt strategies on defect population in ti–6al–4v components manufactured by selective electron beam melting, Materials Characterization 102 (2015) 47–61.

[31] P. Li, Constitutive and failure behaviour in selective laser melted stainless steel for microlattice structures, Materials Science and Engineering: A 622 (2015) 114–120.

[32] M. Braun, I. Ivañez, J. Aranda-Ruiz, Numerical analysis of the dynamic frequency responses of damaged micro-lattice core sandwich plates, The Journal of Strain Analysis for Engineering Design 1-2 (2020) 31–41.

[33] ABAQUS/Standard, Abaqus Standard v6.13 User's Manual, version 6.13 Edition, ABAQUS Inc., Richmond, USA, 2013.

[34] K. Ushijima, W. Cantwell, R. Mines, S. Tsopanos, M. Smith, An investigation into the compressive properties of stainless steel micro-lattice structures, Journal of Sandwich Structures & Materials 13 (3) (2011) 303–329.

[35] M. R. K. Ravari, S. N. Esfahani, M. T. Andani, M. Kadkhodaei, A. Ghaei, H. Karaca, M. Elahinia, On the effects of geometry, defects, and material asymmetry on the mechanical response of shape memory

alloy cellular lattice structures, Smart Materials and Structures 25(2) (2016) 025008.

[36] H. Tankasala, V. Deshpande, N. Fleck, Tensile response of elastoplastic lattices at finite strain, Journal of the Mechanics and Physics of Solids 109 (2017) 307 – 330.

[37] I. Ivañez, L. M. Fernandez-Cañadas, S. Sanchez-Saez, Compressive deformation and energy-absorption capability of aluminium honeycomb core, Composite Structures 174 (2017) 123 – 133. doi:https://doi.org/10.1016/j.compstruct.2017.04.056.